www.czasopisma.pan.pl PAN POLSKA AKADEMIA NAUK www.journals.pan.pl

Arch. Metall. Mater. **68** (2023), 2, 507-516

DOI: https://doi.org/10.24425/amm.2023.142429

MOHAMMAD MEHDI BARJESTEH[1*]

INFLUENCE OF SURFACE ROUGHNESS ON THE HIGH TEMPERATURE /HIGH STRAIN LOW CYCLE FATIGUE BEHAVIOR OF NICKEL-BASED SUPERALLOY RENE®80

Since fatigue cracks nucleate and initiate generally at the surface of the rotary components such as blades and discs, the surface condition is the most important factor affecting the fatigue life. Surface scratches are suitable sites for stress concentrations and therefore the nucleation stage of fatigue cracks will be shortened. In the present work, the influence of surface roughness on the low cycle fatigue life behavior of nickel-based superalloy Rene®80 at the temperature of 900°C was evaluated. Results of low cycle fatigue tests (LCF) under strain-controlled condition at 900°C for $R = \varepsilon_{min}/\varepsilon_{max} = 0$ and strain rate of 2×10^{-3} s^{-1}, at a total strain range of 1.2% showed an inverse relationship between fatigue strength and surface roughness of the specimens. In this study, increasing the surface roughness of Rene®80 from 0.2 µm to 5.4 µm led to the decline in the final LCF life from 127 cycles to 53 cycles which indicated a 58.3% reduction in fatigue life at the same condition. Fractography evaluation also exhibited that fatigue cracks initiated from the notch in the rough specimens, whereas in the smooth specimen fatigue cracks nucleated from the internal imperfections and carbides.

Keywords: Superalloy; Rene®80; Surface roughness; Low cycle fatigue; Fracture surface

1. Introduction

Progress in the reliable assessment of low cycle fatigue life (LCF) of rotary components will decrease overhaul costs of turbojet engines. Polycrystalline cast Rene®80 is a precipitation-strengthened nickel-base superalloy that is employed in the manufacturing process of jet engine turbine blades [1]. The most common failure mechanisms exist in the aviation turbine blade includes different type of fatigues such as high cycle fatigue (HCF), low cycle fatigue (LCF), thermo-mechanical fatigue (TMF) and thermal fatigue (TF) [2, 3]. In the HCF phenomenon, not only residual stresses but also surface roughness, play an effective role in the fatigue life. On the other side, in the LCF condition surface roughness alone is the most important factor. Under high tensile stresses, the residual stresses rapidly relax and so have negligible effect on the LCF life [4]. However, in the literature, LCF has been mentioned as the major failure mode of the aviation turbine blades and wheels [5-8]. Since LCF cracks generally initiate on the part's surface, the surface roughness of a rotating part plays an important role in its LCF strength. Thus, systematic investigation of the effect of the surface roughness on the LCF life can be very beneficial. A review about the related investigations revealed that in spite of some researches on the surface roughness effect on the fatigue life of the steel, titanium and aluminum alloys [9-16], a few evaluations have paid to the effect of this parameter on high temperature/high strain LCF life of the nickel-based superalloy (especially Rene®80). Huang and Ren [4] stated that the residual stress, surface roughness and surface hardening of machined surface were the defining parameters affecting the fatigue performance. The results of their work showed that under the condition of LCF, surface roughness plays the main role and surface hardening has an undesirable effect on the fatigue life of the nickel-based superalloy GH33A, while the residual stress can be neglected because of its relaxation under the applied loads.

HCF tests have been conducted on nickel-based superalloy Inconel 718 specimens with different surface roughness at ambient temperature by Javadi et al. [17]. The summary of this study showed that a valley material component (Mr2), as one of the amplitude distribution parameters, is the most applicable factor for the HCF life of machined specimens.

The effects of machined surface integrity on the LCF life of Inconel 718 at 650°C have been evaluated by Ren et al. [18]. According to the results of this research, the LCF life of the specimens was directly related to its surface roughness. In the scope of turning parameters of the experiments in this

[1] MALEK ASHTAR UNIVERSITY OF TECHNOLOGY (MUT), FACULTY OF MATERIAL AND MANUFACTURING TECHNOLOGIES, TEHRAN 15875-1774, IRAN.

* Corresponding author: mmbarjesteh@yahoo.com

investigation, the cutting speed and feed rate could be selected 80~110 m/min and 0.10~0.12 mm/rev respectively, to attain a better high temperature LCF life.

The LCF response of Waspaloy, a nickel-based superalloy, has been studied by Ardi et al. [19]. In this research, three types of fatigue specimens with various surface roughness have been prepared and then LCF tests have been run. They found that LCF life is sensitive to the height of surface roughness as well as the orientation of the topological features relative to the loading direction.

As seen, there have been a few studies of the effects of surface roughness on the LCF life of nickel-based superalloys. However, in those researches have not been studied about the effect of various kinds of surface roughness on the LCF life of nickel-based superalloy Rene®80. The present study is to search a quantitative correlation between the surface roughness and the LCF life of this superalloy through experiment test. In this research, four different roughness ranges for a similar level of residual stress results are gathered to isolate the effect of roughness on LCF life. This is to make better understanding on how the finishing procedure impacts the LCF life of the aviation/industrial rotary components.

2. Experimental procedure

The alloy selected in the presented work was nickel-based superalloy Rene®80. The main chemical composition of the alloy is provided in Table 1, as determined by a quantometer (spectroscopic) device.

Cylindrical rods, 25 mm in diameter and 120 mm in length, were produced by investment casting. Then, bars were solution-heat treated at 1205°C for 2 h to dissolve primary γ' (strengthening precipitates) and eutectic regions in the as-cast structure and also homogenize the substrate γ phase [20]. However, after solution-heat treated, due to dissolve of the γ' phase, the hardness of Rene 80 will be decreased automatically. This step is the best stage for machining of this superalloy. It should be mentioned that the high value of hardness affects the formation of residual stress on the surface during the machining [4]. After solution heat-treatment, fatigue specimens, 20 mm in diameter and 105 mm length were machined out of the rods using a computerized numerically controlled (CNC) machine as per ASTM E606 (Fig. 1).

LCF specimens were first turned in the same cutting parameters of feed rate (0.35 mm/rev), cutting speed (75 m/min) and depth of cut (0.6). The cutting tool which was used for turning process was bare tungsten carbide.

After the machining process, the surface roughness (R_a – surface roughness in terms of arithmetic average) of the specimens

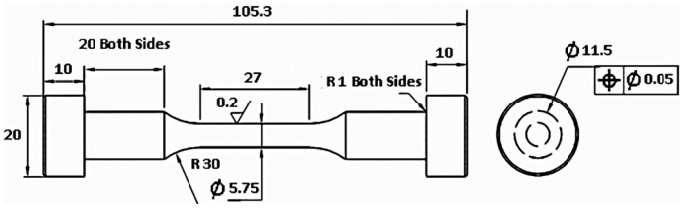

Fig. 1. Dimensions of the standard fatigue test specimen according to ASTM E606 standard [3]

was measured about 5.8-6.5 µm. R_a can indicate both the microscopic geometric features and the height of convex peak [11].

Heat treatment of the fatigue specimens was completed according to GE-C50TF28 (class-A) specification [20,21] to increase the hardness and obtain the optimum mechanical properties. Fig. 2 shows schematically the GE class-A heat treatment.

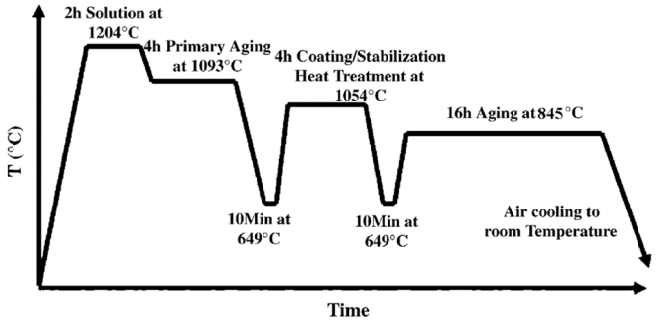

Fig. 2. Schematic illustration showing the heat treatment of nickel-based superalloy Rene®80 [20]

Then, around the gauge area of fatigue specimens were sanded by using #100, #400 and #600 sand papers to obtain an average roughness 5.4 µm, 3.2 µm and 1.5 µm. The LCF test on the standard specimen with 0.2 surface roughness, as Fig. 1, also performed (mechanical polished up to a mirror finish). The surface roughness of the gauge area of fatigue specimens was measured by Mitutoyo roughness profile-meter according to DIN 4768. It should be mentioned that the surface roughness under each condition has been measured from four positions, and the R_a is the average of four data points. Because of the machining parameters for all of the specimen were uniform, therefore the effect of the residual stress can be neglected.

Also, soundness of the fatigue specimens after investment casting and machining have been examined by non-destructive testing (NDT).

For observation of the fractured surface and microstructures, optical microscope (OM – LEICA MEF4A model) and scanning electron microscope (SEM – Zeiss Supra 55 model) equipped with energy dispersive spectroscopy (EDS – Oxford

TABLE 1

The chemical composition of Rene®80 (%wt)

C	Cr	Co	Mo	W	Al	Ti	Fe	Zr	V	B	Si	Mn	Ni
0.16	13.81	9.69	4.23	4.02	3.02	4.87	0.12	0.05	0.05	0.02	0.02	0.03	bal.

model) examinations were performed. The polished samples for OM/SEM characterization were etched in a solution with 10 gr $CuSO_4$, 50 mL HCl and 50 mL H_2O (Marbel solvent).

Phase identification and residual stress measurement were carried out by X-ray diffraction (XRD) method by using an Inel Equinox 6000 with X'Pert High Score Plus v2.0, Cu Kα1 with Graphite monochromator, $2\theta = 10°$ to 90°.

Hardness of alloy (in Vickers scale) was measured by use of automatic Akashi hardness tester equipped with Clemex software, according to ASTM E384.

A computer-controlled tensile testing apparatus (Adelayt Testing Machine model), having a 100 kN load cell, was used for tensile testing of the superalloy Rene®80. Tensile tests were performed with a constant strain rate of 1.6×10^{-4} s^{-1}, in accordance with ASTM E21 standard procedure at 900°C. It should be mentioned that the equipment which was used for tensile test was equipped with an electrical furnace that could apply temperatures up to 1000°C±1. Finally, the LCF test of Rene®80 specimen was carried out in a fatigue component system (servo-hydraulic Instron fatigue test machine-8800 with a maximum capacity of 100 kN). This apparatus equipped with an electrical furnace (1000°C±1) and a high temperature extensometer (Epsilon model) used to perform high temperature fatigue tests in strain control mode. Tests were conducted with a strain ratio $R = \varepsilon_{min}/\varepsilon_{max} = 0$, strain rate of 2×10^{-3} s^{-1}, total strain ($\Delta\mathcal{E}_t$) of 1.2% and tensile-tensile triangular wave at 900 °C according to ASTM E606 standard. Before running the test at high temperature, the specimens were permitted to come to thermal balance for 15 minutes at $\Delta\mathcal{E}_t = 0$.

3. Results and discussion

3.1. Microstructure and hardness of the superalloy Rene®80

The OM micrograph and SEM image of the cast Rene®80 are exhibited in Fig. 3. The microstructure of the Rene®80, after fully heat treatment, consists of the primary (cubic) + secondary (spherical) γ' (strength precipitation) (Fig. 3a), γ matrix phase,

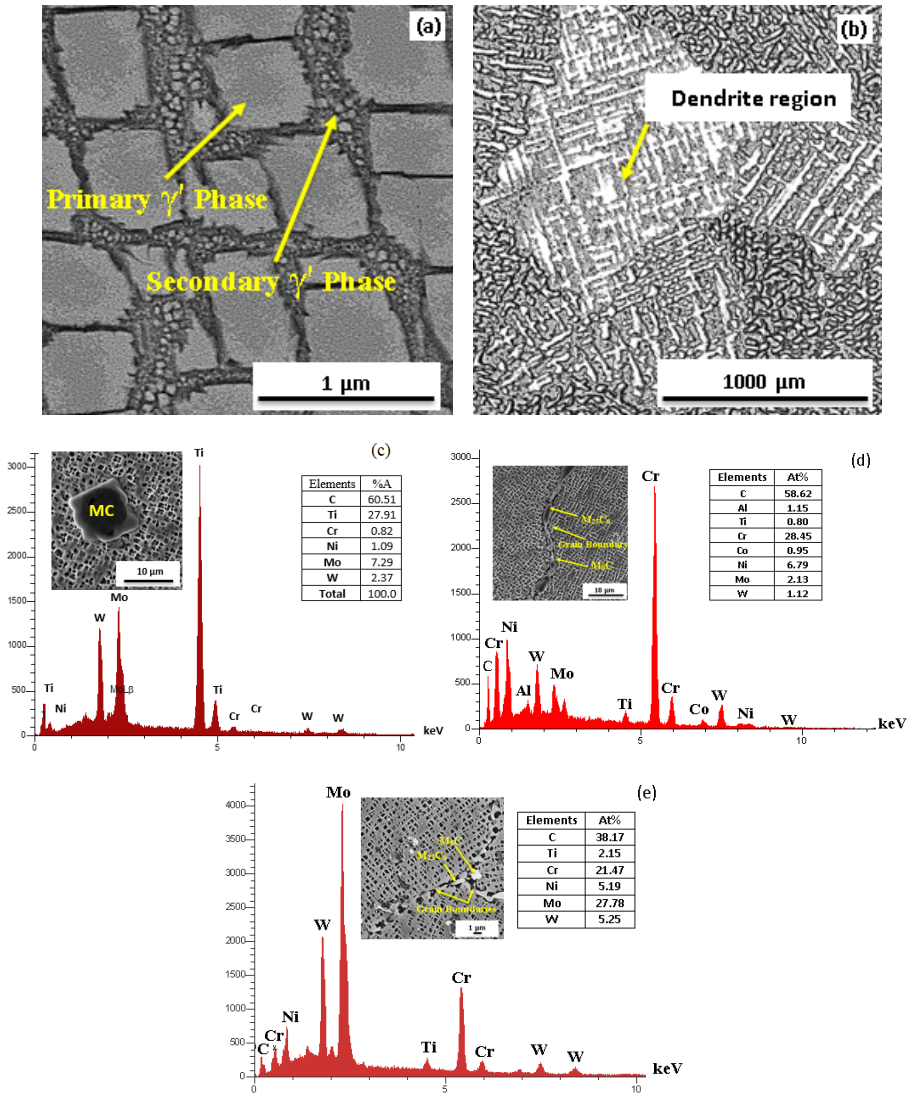

Fig. 3. Nickel-based superalloy Rene®80 (a) SEM image of primary and secondary γ' phases (after fully heat treated); (b) OM micrograph of dendritic region (as cast); (c) EDS result of MC Phase; (d) EDS result of $M_{23}C_6$ Phase and (e) EDS result of M_6C phase

carbides ($M_{23}C_6$ type + MC type + M_6C type) and borides (rich in the Mo, W, Cr, and Ni) that were formed during the aging process [2,20]. The dendrite segregation region of as-cast Rene®80 is also shown in (Fig. 3b). Heavy elements such as W and Mo were segregated at the core of dendrite, while Al and Ti elements enrich in the inter-dendrite region [1, 20]. MC carbides have an FCC structure and create during solidification, with the reaction between reactive element, such as Ti, W, Mo, and C. MC with blocky morphology (inset in Fig. 3c) have an incoherent interface to the matrix. They are found both inside the grains and at the grain boundaries. On the basis of EDS result (Fig. 3c), the formation of Ti-rich MC carbide in the as-cast microstructure of Rene®80 has distinguished. No other carbide of any kinds was determined in the as-cast microstructure. On the other side, the presence of the γ, γ' and MC phases before carrying out the solution heat treatment has also been approved by XRD (Fig. 4), wherein the related peaks to the γ, γ', and MC phases are shown. According to this figure, the related peaks to the γ and γ' phases overlap because of the small difference between their lattice parameters. The presence of these phases in the microstructure of as-cast Rene®80 has also been reported by other researchers [2, 20].

During the heat-treatment or service of cast nickel-based superalloy Rene®80, MC carbides decompose to $M_{23}C_6$ (between 760-980°C) and M_6C (between 815-980°C) carbides as follows: MC + $\gamma \rightarrow M_{23}C_6$ and/or $M_6C + \gamma'$ [20, 22].

$M_{23}C_6$ carbide with the script morphology (see the inset figure in Fig. 3d) and FCC structure, is rich of Cr and precipitates along the grain boundary. On the other hand, M_6C carbides have a complex cubic structure and also precipitate on the grain boundary (see the inset figure in Fig. 3e). Due to M_6C carbides are stable at high temperature, they play an important role in the high temperature strength of superalloys. The probability of formation of M_6C carbides is high in the superalloys containing more than 6% Mo plus W (TABLE 1). The determination of $M_{23}C_6$ and M_6C is difficult because they are very similar to each other. However, due to the difference between chemical compositions of carbides, sometimes the type of carbides can be determined by their colors. For example, it is reported that M_6C carbides appearance in the microstructure brighter than the other carbides [2, 20]. By means of SEM/EDS technology the chemical composition of $M_{23}C_6$ and M_6C carbides have been detected and the results have been shown in Fig. 3d and Fig. 3e, respectively.

Due to segregation of the solute elements in the casting step and formation of large area of dendrite region, the hardness of the alloy after casting was very high and reported 343±20 HV. After the primary aging heat treatment (first precipitation) and fully heat treatment of polycrystalline Rene®80, the values of hardness were measured and reported 278±20 HV and 390±10 HV, respectively. Also, the grain size and the total (primary + secondary) γ' average volume fraction of polycrystalline Rene®80, after fully heat-treatment, were measured and the results were equaled to # 4 (in accordance with ASTM E112-96) and 51-55% (measured with Clemex image analyzer v3.5), respectively. In addition, the average of γ' size was measured about 0.54-0.56 µm. It should be noted that a reduction in the grain size of the alloys lead to the decrease of the surface roughness [6,7].

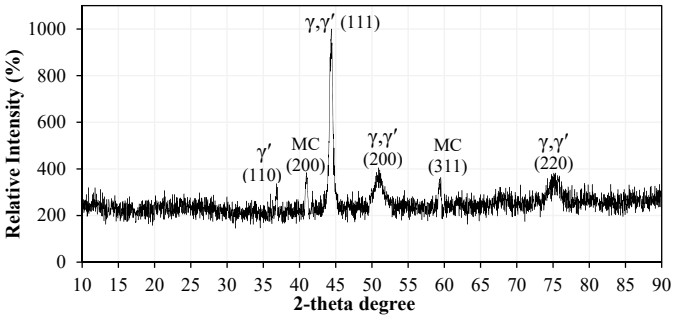

Fig. 4. XRD results of as-cast nickel-based superalloy Rene®80

3.2. Low Cycle Fatigue behavior

The roughness curves of the LCF specimens are shown in Fig. 5. As seen from Fig. 5, the height and depth of the peaks and valleys are within the range of −1 µm to +1 µm for the specimen with roughness *Ra* = 0.2 µm, while this distance are within the range of −20 µm to +20 µm for the specimen with roughness *Ra* = 5.4 µm.

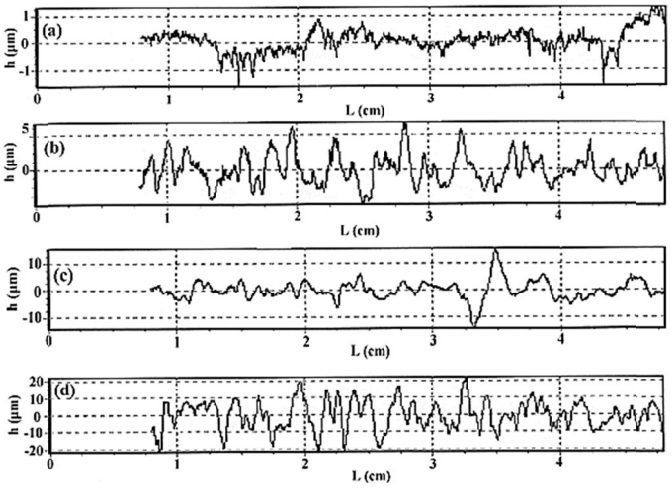

Fig. 5. Roughness curve of Rene®80 (a) *Ra* = 0.2 µm; (b) *Ra* = 1.5 µm; (c) *Ra* = 3.2 µm and (d) *Ra* = 5.4 µm

The severity of surface roughness created in various specimens is shown in Fig. 6. As shown in Fig. 6(a), the surface of the polished LCF specimen is smooth. Some abrasive marks can be observed, on the surface of a specimen with roughness *Ra* = 1.5 µm (Fig 6(b)). Because the roughness affects the reflection of light, an alteration in roughness will seem as a line (beach marks) [23]. These abrasive marks have been created deeply on the surface of specimens with roughness *Ra* = 3.2 µm and *Ra* = 5.4 µm (Fig 6(c) and Fig 6(d)). Depending on the grit paper number used in the process, the desirable roughness on the machined specimens (with roughness *Ra* = 5.8 µm-6.5 µm) can be developed.

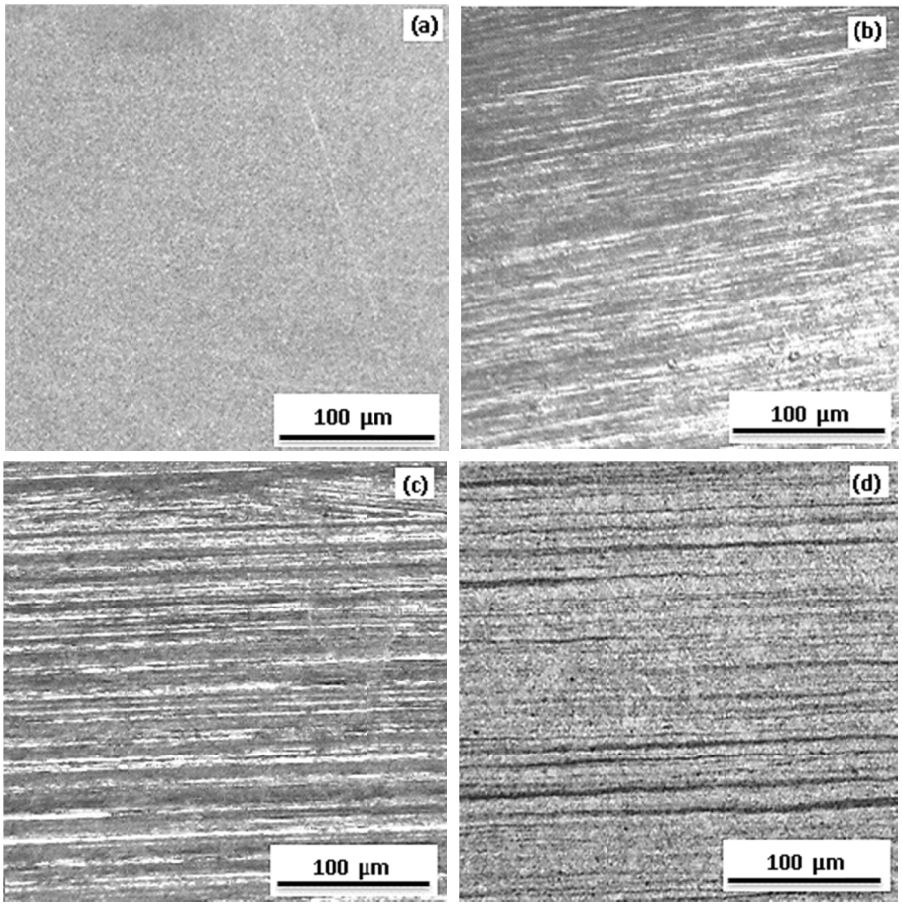

Fig. 6. Micrographs of specimens with different surface roughness. (a) *Ra* = 0.2 µm; (b) *Ra* = 1.5 µm; (c) *Ra* = 3.2 µm and (d) Ra = 5.4 µm

Before the LCF testing, the residual stresses of all specimens have been measured and the results were reported between (–118 MPa)-(–126 MPa). It should be mentioned that the magnitude of residual stress was uniform for all of the specimens.

LCF tests on the Rene®80 specimens with different surface roughness at 900°C and total strain range ($\Delta\mathcal{E}_t = \Delta\mathcal{E}_e + \Delta\mathcal{E}_p$) of 1.2% have been performed and the results have been tabulated in TABLE 2, where $\Delta\mathcal{E}_e$ is the elastic strain, $\Delta\mathcal{E}_p$ is the plastic strain, σ_{max} is maximum cyclic stress, σ_{min} is minimum cyclic stress, N_i is the number of cycles by which the first downfall in the alloy strength is seen (crack nucleation), and N_f is the number of cycles to failure.

Cyclic stress-strain behavior of alloys is depicted to clarify the insufficiency of the monotonic or tensile stress-strain curve in explanation for alloy instabilities caused by cyclic deformations.

In this research, tension test was performed on the standard specimen at 900°C. Monotonic stress-strain curve of nickel-based superalloy Rene®80 at 900°C is shown in Fig 7. The performing of tensile (monotonic stress-strain) test leads to the reduction of low-cycle fatigue test time considerably.

The ultimate tensile strength (UTS) and yield strength (Ys) of this superalloy were measured 610 MPa and 442 MPa, respectively. The percentage of elongation to fracture, was also measured and reported equal to 9.6%. The monotonic tensile yield strength and ultimate strength of superalloy Rene®80 remain unaffected by surface roughness.

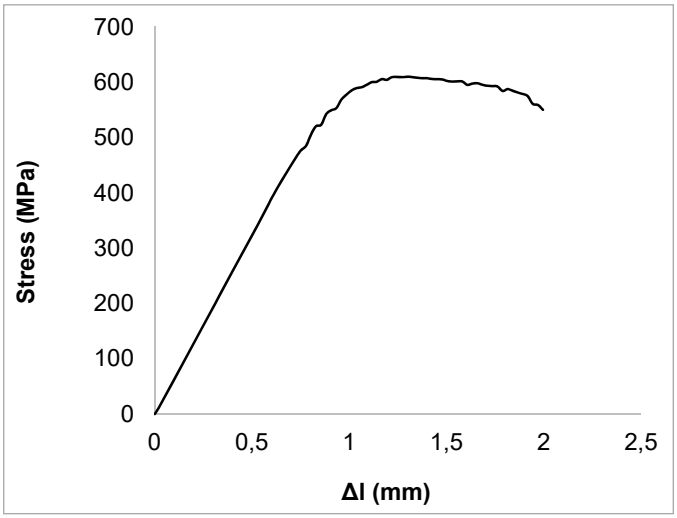

Fig. 7. Monotonic stress-strain curve of Rene®80 at 900°C

As is evident from TABLE 2, there is a direct quantitative correlation between surface roughness and low cycle fatigue behavior. The increase in surface roughness led to the decline of the low cycle fatigue life of Rene®80, at 900°C. In other words, the LCF life has an inverse proportionality with the surface roughness.

As can be observed from TABLE 2, at the total strain of 1.2% and at the temperature of 900°C, the most marked differ-

ence was recorded between Ra = 5.4 μm and Ra = 0.2 μm. The number of cycles tolerated by the specimen with R_a = 0.2 μm (smooth surface) up to failure (N_f) was 127 cycles, while the corresponding number to the specimen with R_a = 5.4 μm (rough surface) was 53 cycles, indicating 58.3 % decrease in the number of tolerated cycles by specimen with rougher surface. The decline in fatigue life that ensues from surface roughness is handily depicted by the ratio $N_f(R)/N_f(S)$, where $N_f(R)$ is the number of cycles to failure for a specimen with roughness R (R_a = 5.4 μm), and N_f(S) is the fatigue life of a specimen with a smooth surface (R_a = 0.2 μm). This quantity was calculated 0.42 (53/127) in this study which indicated 58% reduction in fatigue life of rough specimen. Besides, the results which are inserted in TABLE 2 show that the ratio (Ni/Nf) is greatly affected by surface roughness condition. This ratio for R_a = 0.2, 1.5, 3.4 and 5.4 was calculated 0.93, 0.9, 0.83 and 0.8, respectively. This parameter show that the crack initiated in the rougher specimen sooner than smooth specimen.

TABLE 2

Results of low-cycle fatigue test on Rene®80 specimens with different surface roughness ($\Delta\mathcal{E}_t$ (%) = 1.2, R = 0, $\dot{\mathcal{E}} = 2\times10^{-3}$ s^{-1}, T = 900°C)

Specimens surface roughness R_a (μm)	σ_{max} (MPa)	σ_{min} (MPa)	N_i	N_f
0.2	719.2	–412.1	118	127
	710.8	–415.6	111	119
1.5	727.4	–429.4	103	114
	730.6	–434.2	100	109
3.2	755.8	–452.7	60	72
	759.5	–457.2	56	68
5.4	776.1	–469.6	43	53
	781	–503.6	38	48

Fig. 8 shows the stress-strain hysteresis loops, at the first cycle, at $\Delta\mathcal{E}_t$ (%) = 1.2 and at the temperature of 900°C for the specimens with Ra = 0.2 and Ra = 5.4. The combined output of the extensometer and load cell supplied the strain-cycle trace from which the hysteresis loop is created. The area of the hysteresis loop is equal to the work performed or the energy loss per cycle [24]. There are a few slip systems, at the first cycle N_i, and dislocations are accumulated in the γ phase due to its lower strength compared to the γ' phase. Increasing the number of cycles during fatigue test, could lead to an increase in the quantity of slip systems, therefore, the concentration of dislocations is also increased. Upon dislocation-dislocation interactions, the strength of the Rene®80 reduces and the specimen is neglected at the N_f cycle [2, 25].

As seen from TABLE 2 and Fig. 8, the specimen with R_a = 5.4 μm has tolerated the maximum stress range ($\Delta\sigma = \sigma_{max} - \sigma_{min}$). This value is equal to 1245.7 MPa. Also, the minimum stress range belongs to the specimen with R_a = 0.2 μm which equals to 1131.3. In other words, the smoothness specimen which tolerated a lower stress level, indicating improved fatigue life. Fig. 8 also shows that the smoothness specimen (Ra = 0.2 μm) tolerated a lower plastic strain in comparison with the rough specimen (Ra = 5.4 μm).

Tan et al. [12] mentioned that the geometrical notch stress concentration factor (K_t) caused by surface roughness is greater for the rough surface specimens than smooth surfaces. The stress concentration factor can be characterized as $K_t = 1 + 2[\gamma (R_z/\rho)]^{1/2}$ [10,23]. Where γ equals to one, R_z is the maximum height of the profile and ρ is the actual profile valley radius of the surface texture. The rougher specimens have a larger R_z and a lower ρ. Thus, it can be undoubtedly resulted that the quantity of K_t is high in the rougher specimens. The stress amplitude in the notch can be obtained from the multiplication of stress concentration factor by strain amplitude [10].

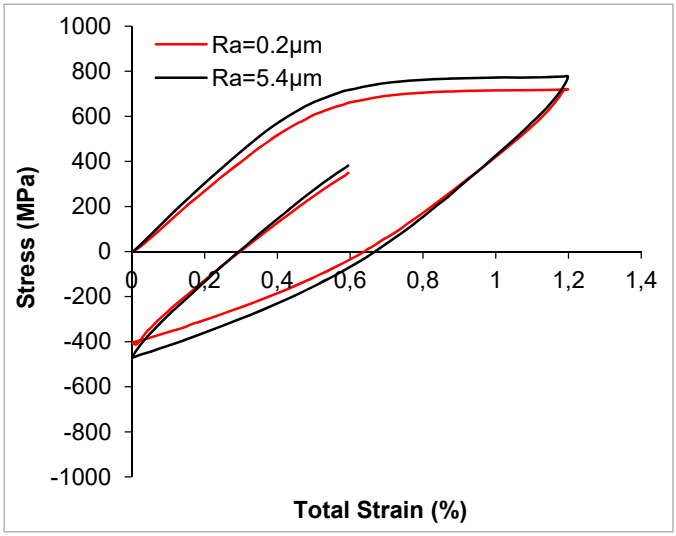

Fig. 8. Hysteresis stress-strain loop at the first cycle for Rene®80 with the surface roughness of Ra = 0.2 μm and Ra = 5.4 μm (T = 900°C and $\Delta\mathcal{E}_t$ (%) = 1.2).

According to the mentioned explanations, during LCF test, greater local stress-strain field was created in the specimen with high surface roughness. Because of the presence of this high stress level, the decrease of endurance limit was occurred and as a result, fatigue life was reduced in this specimen. In other words, stress concentrations give rise to crack initiation. In most cases, fatigue cracks initiate in regions of stress concentration, such as scratches, notches and other flaws of surfaces where the cyclic plastic deformations are higher than average. However, cracks do reduce the load-bearing area of the specimen and hence decline the fatigue strength of the alloy. Therefore, it would be anticipated that any measures that reduce stress concentration can guide to meliorated fatigue life. As stated earlier, surface roughness is described as a preferred location for crack nucleation. The fatigue life is usually divided by two sections: (1) crack initiation and (2) crack growth [23,24]. However, a slip step penetrates through a free surface and roughness on the surface is a favorable condition for crack initiation period. A very applicable reason is the inhomogeneous stress distribution (stress concentration) due to geometric discontinuity (surface roughness). After cracks initiation period, the micro-cracks connect together and create

an inhomogeneous stress distribution on a micro-level, with a stress concentration at the tip of the micro-cracks. As a result, more than one slip system may be activated [23,24]. In general, micro-cracks grow perpendicular to the loading direction. The presence of micro-cracks on the surface also lead to decrease in the load bearing cross section and therefore the remaining surface of the specimen tolerated a higher stress. It means that increasing surface roughness maximizes, local stress raisers. Therefore, the specimen with higher quantity of surface roughness (Ra = 5.4 μm) failed at the shortest time.

3.3. Fracture surface morphology evaluation

The fracture surfaces of the specimens after LCF test were evaluated by scanning electron microscope. All of the LCF specimens showed fatigue striations; examples, at the different magnification, are presented in Fig. 9. The largest portion of a fatigue fracture consists of crack growth. The fracture morphology of this step may show beach lines known as stable fatigue striations. Each striation is produced by one cycle of stress. The fatigue striations are normal to the crack propagation path ascertained far from crack initiation location [2,23].

As noted earlier, the surface scratches are eligible sites of crack initiation, and therefore, they can effectively destroy the LCF property of the alloy. Surface roughness also plays the role of notch on the surface of the specimens, therefore, in the rough specimen, the highest stress took place at the notch and each notch will be a potential location for micro-cracks. It is also reported in the literature [23,25] that a surface roughness results, leading to the stress concentrations at the grain boundaries. This stress concentration can finally make de-cohesion along the grain boundary. On the other side, at high-temperature LCF, the grain boundary will be oxidized [26]. Such results (stress concentration + grain boundary oxidation) propose a weakening of grain boundaries and consequent formation of preferential crack paths along the boundaries.

It has been reported that surface roughness has directly affected on oxidation resistance of the superalloys. A reduction in surface roughness, lead to an increase in oxidation resistance

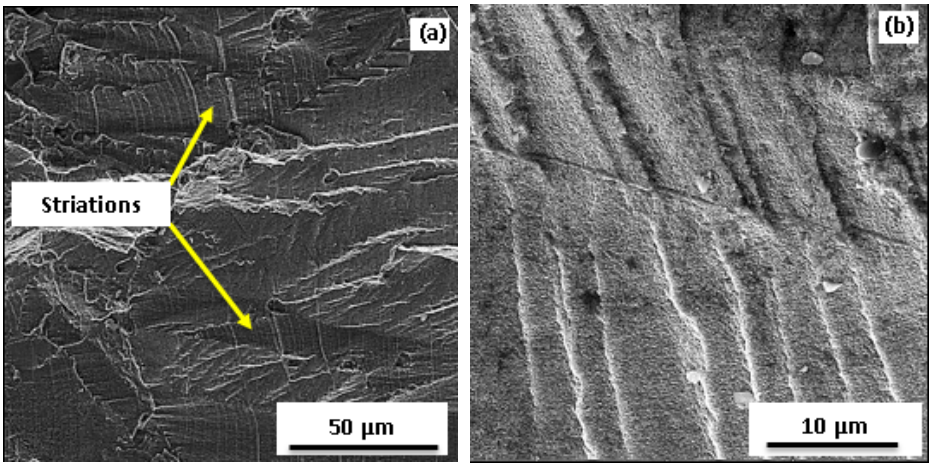

Fig. 9. SEM (secondary electron) images of (a) fatigue striations (Ra = 0.2 μm); (b) fatigue striations at higher magnification

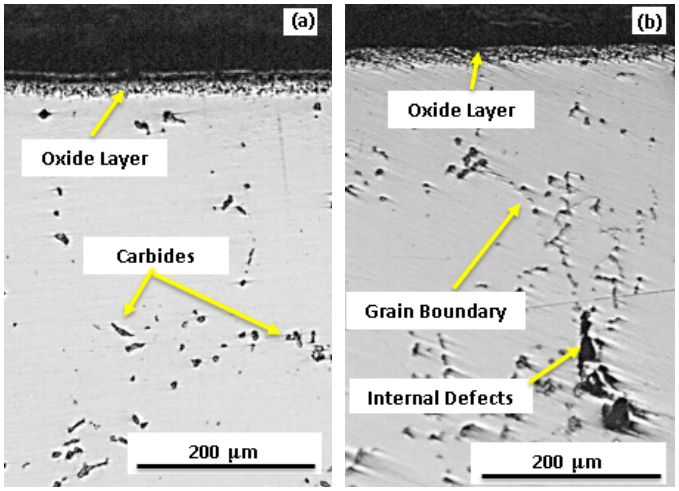

Fig. 10. Surface of the specimen after LCF test at T = 900°C, R = 0, $\Delta\mathcal{E}_t$ = 1.2% (a) Rough specimen (R_a = 5.4 μm); (b) smooth specimen (R_a = 0.2 μm)

[27-29]. The outward diffusion of aluminum grows with the rise of surface roughness. Hence, the level of aluminum concentration reduces with the enhancement of surface roughness when the selective oxidation of aluminum takes place to produce a protective α-Al_2O_3 scale [28]. Thus, it can be expected to record the minimum oxidation resistance for the specimen with high level of surface roughness (R_a = 5.4 μm). Thick oxide layer (≈25.64 μm) which has been formed on the surface of a rough specimen (R_a = 5.4 μm) during the LCF test (Fig. 10(a)) as compared to thin oxide layer (≈ 15.4 μm) on the surface of the smooth specimen (R_a = 0.2 μm) (Fig. 10(b)), has high contents of nickel, aluminum and titanium.

These elements are the main elements which exist in the composition of γ' (Ni_3 (Al, Ti)) phase (strengthening precipitates). Thus, the surface of the bare alloy will be denuded of γ' phase at high temperature [26]. Due to the depletion of the near-surface area from γ', the alloy strength decreases, providing

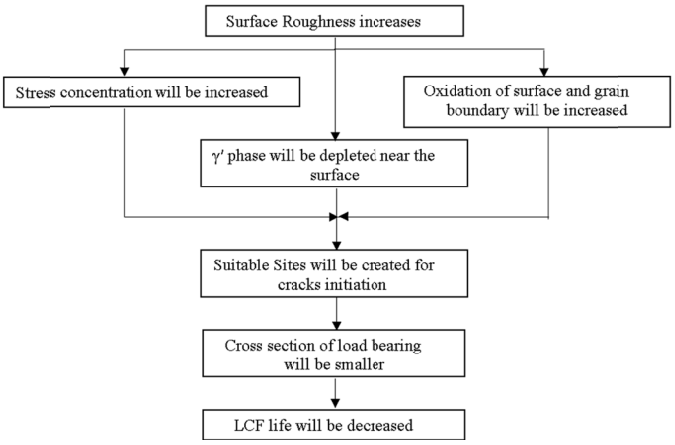

Fig. 11. Flow chart showing the effect of surface roughness increasing on LCF life

a basis for more micro-crack initiation. In addition, in the present study, due to high strain (1.2%), breakage of the brittle oxide layer will be occurred easily and therefore, the fresh surface of alloy will oxide frequently. Finally, the thick oxide layer will be formed on the surface. Oxidation decreases fatigue life by means of affecting crack initiation and growth behavior at high temperature as 900°C. The formation of a thick oxide layer on the surface of bare nickel-based superalloy during the low cycle fatigue test has also been reported by other researchers [30,31].

Flow chart indicating the reasons for LCF life reduction due to surface roughness increasing is shown in Fig. 11.

Although crack nucleated from the outer surface of the specimens with R_a = 5.4 μm, 3.2 μm and 1.5 μm (Fig. 12(a) and (b)), crack initiated from the inner imperfections in the smooth specimen (R_a = 0.2 μm) (Fig. 12(d)).

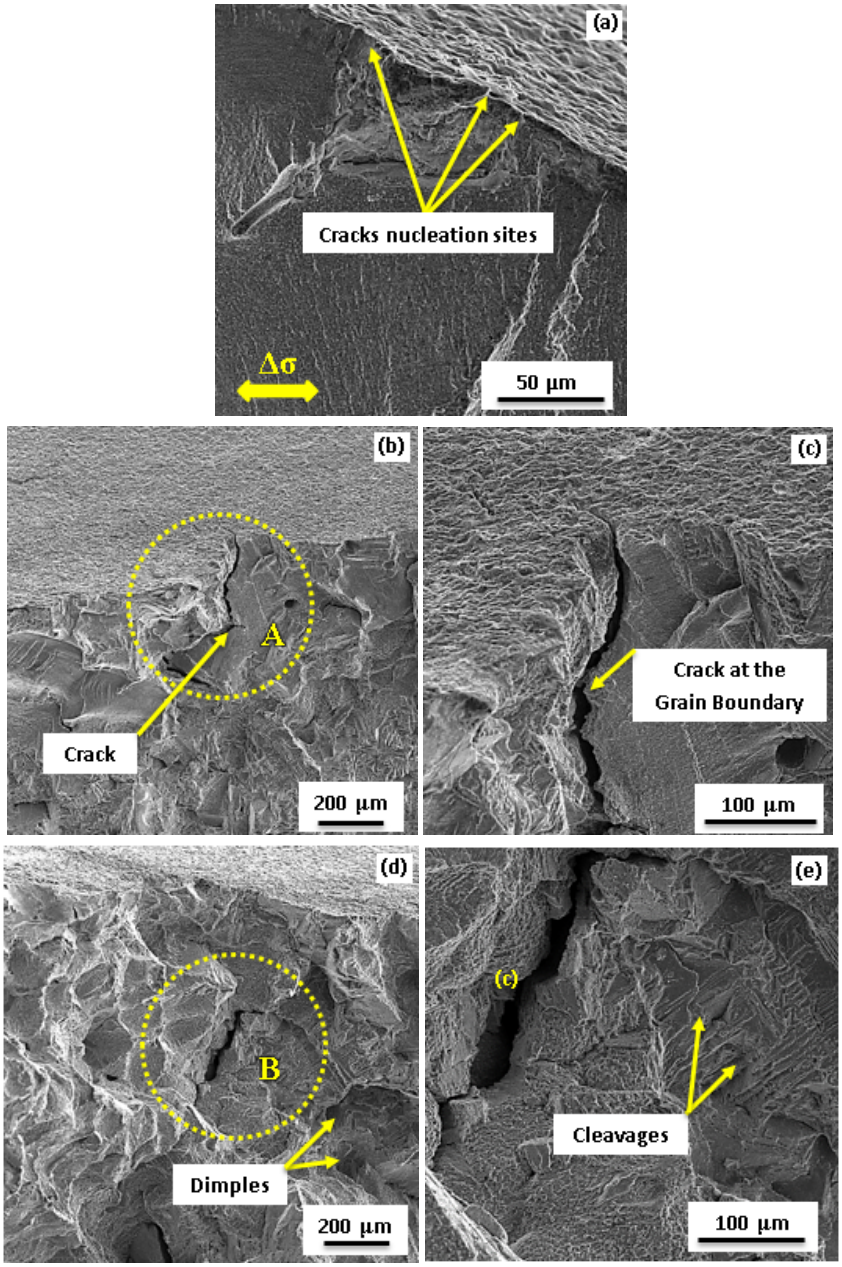

Fig. 12. SEM (secondary electron) images of fracture surface of (a) LCF specimen with *Ra* = 5.4 μm; (b) LCF specimen with *Ra* = 3.2 μm; (c) Magnified view of "A" area; (d) LCF specimen with *Ra* =0.2 μm; (e) Magnified view of "B" area (T = 900°C, R = 0, $\Delta\varepsilon t$ = 1.2%).

The LCF failure in the as-polished (smooth) specimens initiated from internal defects (Fig. 10(b) and Fig. 12(d)) or carbides. The EDS analysis indicated that TiC was the carbide type which crack initiated from it (Fig. 13).

It should be mentioned that no difference was evident from the fracture surface of the specimens with R_a = 3.2 μm and 1.5 μm. On the other hand, the number of initiation sites is more for the specimen with a surface roughness of 5.4 μm (Fig. 12(a)) than for that with a surface roughness of 3.2 μm and 1.5 μm (Fig. 12(b)). This phenomenon reduces the load bearing cross section; therefore, the specimen cannot withstand with the applied stress anymore and finally, LCF life of a rough specimen will be declined.

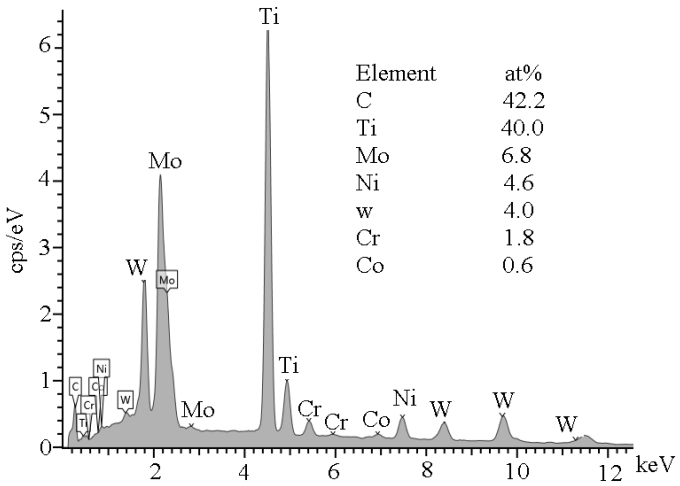

Fig. 13. EDS analysis at Point C of Fig. 12(e)

The crack propagation properties, such as crack shape (sharp and inclined cracks propagate in the perpendicular direction from the loading direction), for all of the specimens are almost the same. Therefore, it could be concluded that the difference between the LCF lives of the specimens with different surface roughness is independent of the crack propagation. It means that even if surface roughness is a cause of crack initiation, its influence on crack growth is less evaluative. In other words, although the surface roughness accelerates the fatigue crack initiation, there is no effect on the fatigue crack propagation. This result is in accordance with the result of Fujimura et al. research [9].

Also, fracture surface analysis indicates a mixed mode of ductile (dimples) and brittle (cleavage) failure under cyclic loading at T = 900°C and $\Delta\mathcal{E}_t$ (%) = 1.2 in all of the specimens. Cleavage area which is more related to the celerity of fracturing [23], was observed more in the specimen with Ra = 5.4 μm than the other specimens. The cleavage and dimples morphology have been shown in Fig. 12(d) and Fig. 12(e).

It was clarified by the results of this study that surface quality control of the rotating parts is very important. This quality control procedure should be accurately implemented to prevent surface defects or roughness. Otherwise, the fatigue life will be decreased several times less than standard smooth specimen data. Therefore, the surface roughness is a very significant concept in the design calculations. Extreme care must be taken to avoid or to remove machining marks or scratches, normal to the loading direction.

4. Conclusions

In this work, low cycle fatigue tests with different surface roughness states of nickel-based superalloy Rene®80, at (T = 900°C, R = 0, $\Delta\mathcal{E}_t$ = 1.2%) were carried out. The effect of magnitude of surface roughness on LCF life was evaluated. The major results are as follows:

1 – The LCF data of Rene®80 alloy regarding the surface roughness indicate that the surface roughness has an important influence on the fatigue life. The specimens with a smaller surface roughness have a longer LCF life.

2 – The LCF life reduction for the specimens with surface roughness of 1.5 μm, 3.2 μm and 5.4 μm compared to the smooth specimen (R_a = 0.2 μm) is determined 10.2%, 43.3% and 58.3%, respectively. In other words, decreasing the surface roughness from 5.4 μm to 0.2 μm led to the improvement in the final LCF life of Rene®80 from 53 cycles to 127 cycles, which show about 42% betterment in the LCF life.

3 – The fracture surface analysis exhibit that, although cracks nucleated from surface scratches in the rough specimen (Ra = 1.5 μm, Ra = 3.2 μm and Ra = 5.4 μm) cracks initiated from internal defects and carbides in the smooth specimen (Ra = 0.2 μm). On the other hand, the crack nucleation sites on the surface of the specimen with Ra = 5.4 μm were more than the other specimens.

REFERENCES

[1] M.M. Barjesteh, S.M. Abbasi, K. Zangeneh-Madar, K. Shirvani, Mater. Chem. and Phys. **227**, 46-55 (2019).

[2] S. Zhang, D. Zhao, Aerospace Materials Handbook, CRC Press Taylor & Francis Group 2013.

[3] M.M. Barjesteh, K. Zangeneh-Madar, S.M. Abbasi, K. Shirvani, J. Min. Metall. B. **55** (2), 235-251 (2019).

[4] Q. Huang, J. X. Ren, Int. J. Fatigue. **13** (4), 322-326 (1991).

[5] P. Zhang, Q. Zhu, G. Chen, H. Qin, C. Materials **8**, 6179-6194 (2015).

[6] H. Buhl (1st Ed.), Advanced Aerospace Materials, Springer-Verlag Berlin 1992.

[7] J. Schijve, Fatigue of Structures and Materials, Kluwer Academic Publishers 2004.

[8] I.S. Kim, B.G. Choi, J.E. Jung, J. Do, C.Y. Jo, Mater. Charact. **106**, 375-381 (2015).

[9] N. Fujimura, T. Nakamura, H. Oguma, J. Solid Mech. Mater. Eng. **7** (3), 372-380 (2013).

[10] W.L. Xiao, H.B. Chen, Y. Yin, Key Eng. Mater. **525-526**, 417-420 (2013).

[11] Y. Wang, E.I. Meletis, H. Huang, Int. J. Fatigue. **48**, 280-288 (2013).
[12] L. Tan, C. Yao, D. Zhang, J. Ren, Z. Zhou, J. Zhang, Int. J. Fatigue. **136**, 105630 (2020).
[13] Z.G. Liu, T.I. Wong, W. Huang, N. Sridhar, S.J. Wang, Acta Metall. Sin. (Engl. Lett.). **30** (7), 630-640 (2017).
[14] J. Peguesa, M. Roach. R.S. Williamson. N.Shamsaei, Int. J. Fatigue. **116**, 543-552 (2018).
[15] A. Cox, S. Herbert, J.-P. Villain-Chastre, S. Turner, M. Jackson, Int. J. Fatigue. **124**, 26-33 (2019).
[16] T. Gao 1, Z. Sun, H. Xue, E. Bayraktar, Z. Qin, B. Li, H. Zhang, Metals. **10**, 1507-1522 (2020).
[17] H. Javadi, W. Jomaa, D. Texier, M. Brochu, P. Bocher, Solid State Phenom. **258**, 306-309 (2017).
[18] X. Ren, Z. Liu, X. Liang, P. Cui, Materials, **14**, 2428-2444 (2021).
[19] D.T. Ardi, Y.G. Li, K.H.K. Chan, M.R. Bache, J. Mater. Eng. Perform. **23** (10), 3657-3665 (2014).
[20] J. Safari, S. Nategh, J. Mater. Process Technol. **176**, 240-250 (2006).
[21] GE Aircraft Engines specification, C50TF28, USA 1996.
[22] B. Chmiela, B. Koscielniak, J. Cwajna, Arch. Metall. Mater. **62** (1), 241-245 (2017).
[23] A. R. Rosenfield, ASM International, Fracture Mechanics in Failure Analysis section, Fatigue and Fracture, Volume 19, Materials Park 1996.
[24] F.C. Campbell, Fatigue and Fracture: Understanding the Basics, Materials Park 2012.
[25] P. R. Bhowal1, D. Stolz, A. M. Wusatowska-Sarnek, R. Montero, Superalloys, 417-423 (2008).
[26] K. Rahmani, S. Nategh, Mater. Sci. Eng. A. **494** (1), 385-390 (2008).
[27] D.K. Das, Prog. Mater. Sci. **58**, 151-182 (2013).
[28] H. Pei, Z. Wen, Z. Li, Y. Zhang, Z. Yue, Appl. Surf. Sci. **440**, 790-803 (2018).
[29] C. Cheng, Y. Hu, T. Cao, L. Zhang, Y. W. Zhu, J. Zhao, Corros. Sci. **176**, 108942 (2020).
[30] Z.D. Fan, D. Wang, C. Liu, G. Zhang, J. Shen, L.H. Lou, J. Zhang, Acta Metall. Sin. (Engl. Lett.). **30** (9), 878-886 (2017).
[31] N. Tada, R. Ohtani, A. Wad, J. Soc. Mat. Sci., Japan **52** (2), 132-138 (2003).